



## Article

# Estimating Tree Defects with Point Clouds Developed from Active and Passive Sensors

Carli J. Morgan<sup>1</sup>, Matthew Powers<sup>1</sup> and Bogdan M. Strimbu<sup>1,2,\*</sup>

- <sup>1</sup> Department of Forest Engineering, Resources and Management, Oregon State University, Corvallis, OR 97331, USA; carli.morgan@oregonstate.edu (C.J.M.); matthew.powers@oregonstate.edu (M.P.)  
<sup>2</sup> Faculty of Silviculture and Forest Engineering, Transilvania University of Brasov, 500036 Brasov, Romania  
\* Correspondence: bogdan.strimbu@oregonstate.edu; Tel.: +1-541-737-1604

**Abstract:** Traditional inventories require large investments of resources and a trained workforce to measure tree sizes and characteristics that affect wood quality and value, such as the presence of defects and damages. Handheld light detection and ranging (LiDAR) and photogrammetric point clouds developed using Structure from Motion (SfM) algorithms achieved promising results in tree detection and dimensional measurements. However, few studies have utilized handheld LiDAR or SfM to assess tree defects or damages. We used a Samsung Galaxy S7 smartphone camera to photograph trees and create digital models using SfM, and a handheld GeoSLAM Zeb Horizon to create LiDAR point cloud models of some of the main tree species from the Pacific Northwest. We compared measurements of damage count and damage length obtained from handheld LiDAR, SfM photogrammetry, and traditional field methods using linear mixed-effects models. The field method recorded nearly twice as many damages per tree as the handheld LiDAR and SfM methods, but there was no evidence that damage length measurements varied between the three survey methods. Lower damage counts derived from LiDAR and SfM were likely driven by the limited point cloud reconstructions of the upper stems, as usable tree heights were achieved, on average, at 13.6 m for LiDAR and 9.3 m for SfM, even though mean field-measured tree heights was 31.2 m. Our results suggest that handheld LiDAR and SfM approaches show potential for detection and measurement of tree damages, at least on the lower stem.

**Keywords:** tree defect; structure from motion; handheld LiDAR; photogrammetry; forest inventory



**Citation:** Morgan, C.J.; Powers, M.; Strimbu, B.M. Estimating Tree Defects with Point Clouds Developed from Active and Passive Sensors. *Remote Sens.* **2022**, *14*, 1938. <https://doi.org/10.3390/rs14081938>

Academic Editors: Alexandru Isar and Francois Girard

Received: 21 January 2022

Accepted: 13 April 2022

Published: 17 April 2022

**Publisher's Note:** MDPI stays neutral with regard to jurisdictional claims in published maps and institutional affiliations.



**Copyright:** © 2022 by the authors. Licensee MDPI, Basel, Switzerland. This article is an open access article distributed under the terms and conditions of the Creative Commons Attribution (CC BY) license (<https://creativecommons.org/licenses/by/4.0/>).

## 1. Introduction

Periodic resource assessments are routinely used to estimate timber volume and value, tree growth rates, carbon storage, forest health status, species, coarse woody debris, fuel loading, and more. Historically, qualified cruisers (i.e., trained forestry measurement specialists) executed field forest inventories using specialized tools, manual measurements, and visual estimation. Forest inventories are typically plot-based samples of a predefined area and, in some cases, repeated on a 5- to 15-year basis.

Traditional inventories require a trained workforce and a substantial amount of time. Additionally, sample-based inventories may not fully capture the diversity of a forest stand. Typically, plots capture less than 20% of the forested area in a stand [1]. This can be problematic for diverse, uneven-aged stands that are not homogenous. Additionally, field measurements rely on the expertise of the practitioner and are prone to error [2,3].

Recent developments in the field of remote sensing are revolutionizing the way forest inventory data are gathered and analyzed. Remote sensing involves the use of passive or active sensors to capture reflected energy, which, in turn, can be used to describe or measure attributes of the targeted object. The most prevalent platforms for collecting tree data are satellites, airplanes, unmanned aerial systems (UASs), and ground-based (terrestrial) sensors (i.e., automotive or hand-held).

One of the most promising applications of remote sensing includes the use of light detection and ranging (LiDAR). LiDAR is an active remote sensing technique that uses laser pulses to scan the environment. Current LiDAR devices send thousands, even millions, of laser pulses per second, which are reflected back by the forest ecosystem. The sensor either records the time it takes for an individual pulse of light to be reflected back or the phase shift between the sent and received pulse and, using a series of algorithms and angle measurements, computes the location of the return.

An emerging application of terrestrial LiDAR is handheld LiDAR, which has achieved promising results in tree detection and measuring diameter at breast height (DBH) and height, while decreasing the amount of time, equipment, expertise, and cost to collect remote sensing data [4–6]. Handheld LiDAR scanners have a maximum range of approximately 100 m and can emit upwards of 300,000 laser pulses per second [7]. Studies using this new generation of mobile scanners were able to detect 77–96% of trees over 5-cm DBH [5,6], with an RMSE for measuring DBH from 0.9–2.3 cm. Handheld laser scanners can measure tree heights up to 7–33 m with an RMSE of 0.4–1.4 m [5,6].

Another remote sensing technology frequently applied to forest inventory is photogrammetry [8,9]. Photogrammetry uses a camera (typically equipped with a red-green-blue sensor) to capture solar light energy reflected off objects. Common platforms for photogrammetry are satellites, aerial carriers (i.e., helicopter, fixed-wing aircraft, or UAS), and terrestrial carriers (i.e., tripods, vehicles, or humans).

The last two decades saw the emergence of a new photogrammetric application, namely Structure from Motion (SfM), which utilizes moving camera positions, overlapping photo images, and computer-vision techniques to reconstruct 3D models of objects. Recently, several studies employed terrestrial SfM to measure diameter at breast height (DBH), tree position, height, and stem curve. The results suggested that DBH could be measured within 0.9–6.8 cm RMSE, depending on the equipment and methods used [10–16], the positions with 0.16–0.20 m RMSE [13], whereas the average total tree height varies from 4.3–20 m, depending on the estimated stem completeness [13,15]. Stem curves can be estimated with sub-centimeter accuracy up to approximately 3 m above ground level [15].

In addition to the size and location of the trees, a forest inventory records the defects present throughout the forest stand. Defects are tree damages caused by structural deformities, animal browse, mechanical damage, insects and disease activity, or weather events, to list just a few. Including defect assessment in a forest inventory directly relates to quantifying forest attributes, such as net timber volume and value, insect and disease activity, and wildlife habitat. Traditionally, a tree defect is assessed in the field using hand-held forestry tools and/or visual estimation. Typically, a cruiser identifies the presence or absence of damage, records the source, and quantifies the amount of the tree stem affected by the damage [17].

To date, very few, if any, studies have utilized handheld LiDAR or SfM to assess tree defect. There are a small number of related studies conducted with terrestrial laser scanning (TLS), which may serve as an analog for handheld LiDAR. Using TLS, small log defects can be detected down to ~0.5 cm in size [18]. Additionally, some defects, such as branch scars, can be measured with approximately 6–9 mm accuracy, compared to manual measurements [19]. Studies focused on taper, lean, and sweep based on TLS reached conflicting results for taper, whereas lean angle was measured within ~2°, and sweep with approximately 1–2 cm/m accuracy [20]. Since handheld LiDAR and TLS use similar technologies, we expect handheld LiDAR to have utility in assessing tree defect. There is not a functional analog for SfM photogrammetry; however, the technology has proven useful in measuring DBH, tree position, height, and stem curve [10–16]. Therefore, we expect SfM to have utility in assessing and quantifying tree damage.

Although handheld LiDAR and SfM can provide precise estimates of basic tree measurements, there is no clear evidence that tree quality can be assessed using point clouds. Therefore, the main objective of our study is to assess the ability of handheld LiDAR and SfM photogrammetry to identify and estimate the magnitude of tree defects. We con-

sider a defect any damage that reduces the ability of a tree to thrive and produce quality wood products, such as those caused by structural deformities, animal browse, mechanical damage, insects and disease activity, weather events, etc. The necessity to estimate the magnitude of the defects is based on the relationship between stem quality and many forest management attributes, such as net timber volume and value, insect and disease activity, and wildlife habitat. Consequently, the research questions guiding the present study are:

- (1) Can SfM and handheld LiDAR accurately detect the tree damages?
- (2) Can SfM and handheld LiDAR accurately determine the magnitude of tree damage?

## 2. Materials and Methods

### 2.1. Study Area

The study was conducted on the McDonald Research Forest, managed by Oregon State University's College of Forestry (Figure 1). The site is located north of Corvallis, Oregon, and representative of inland Coast Range forests. The temperature ranges from approximately 0.8–28.1 °C, with a mean annual temperature of 11.4 °C. Mean annual precipitation for the region is 108.5 cm (NOAA National Climate Data Center, Asheville, NC, USA). Elevation for the forest stand ranges from 215 to 400 m, and the research sites face a southeasterly direction. The terrain ranges from 15 to 55% slope, with an average slope of 15% within the research plots.

The forest stand is approximately 160 years old. The tree species composition consists of second-growth Douglas-fir (*Pseudotsuga menziesii*) with minor components of bigleaf maple (*Acer macrophyllum*), grand fir (*Abies grandis*), Oregon ash (*Fraxinus latifolia*), and Oregon white oak (*Quercus garryana*). The mean diameter-at-breast-height across the study area was 54.3 cm. The mean height was 31.7 m, with approximately 288 trees per hectare.

### 2.2. Data Collection

#### 2.2.1. Field Inventory for Visual Assessment of Damages

We conducted field measurements in June and August of 2019. To ensure tree damages were present, we selected a mature forest stand with a high frequency of tree defect for sampling. We measured all live trees with diameter-at-breast-height (DBH) greater than 12.7 cm within three, 400 m<sup>2</sup> (i.e., 11.3 m radius) plots within the stand. We recorded species, DBH, total height, damage type, damage length, and damage location for each tree (Table 1). We visually estimated the location of each incidence of damage on the stem by dividing the total tree height into thirds to represent a bottom, middle, and top portion of the stem. For each observed incidence of damage on the tree, we recorded a two-digit damage code reflecting the type of damage and a one-digit location code reflecting the position on the stem (Table 1). For example, a tree with a 'spike knot' would have a damage code of '98'. If the spike knot occurred in the middle third of the tree stem, we recorded a damage location of '2'. The length of the damage was visually estimated to the nearest 0.3 m. Finally, we summed the total number of damages per tree to create a damage count variable. A total of 35 trees were measured across the three plots: 25 Douglas-fir, 7 bigleaf maple, 1 grand fir, 1 Oregon ash, and 1 Oregon white oak.

#### 2.2.2. Photogrammetric Imagery and Point Cloud Generation

In June and August of 2019, we acquired the images needed for the generation of photogrammetric point clouds using SfM. To facilitate image capture and minimize occlusion, understory shrubs and tree saplings were felled and removed from the three plots. Some coarse woody debris remained but did not obscure the target trees. Photos were captured with a Samsung Galaxy S7 (SM-G930V, Suwon-si, South Korea) smartphone. We took handheld photos with vertical (portrait) orientation of the smartphone camera using the following settings:

- Focal length: 4 mm;
- Maximum aperture: 153;
- 35 mm focal length: 26;

- Flash: no flash;
- Exposure time: automatic, variable;
- ISO speed: automatic, variable;
- File type: .jpg, converted to tiff.

To ensure consistency of the methodology and results, we took photos in a circular pattern around each individual tree stem within the three fixed-radius plots, striving for at least 90% overlap between photos, similarly to Fang and Strimbu [8]. Photos were captured approximately every meter. Distance to the target tree varied; however, most photos were captured approximately 5 to 10 m from the tree. The number of photos per tree varied from 25 to 48 photos. No targets or control points were placed within the scene. All images were collected in the summer of 2019.

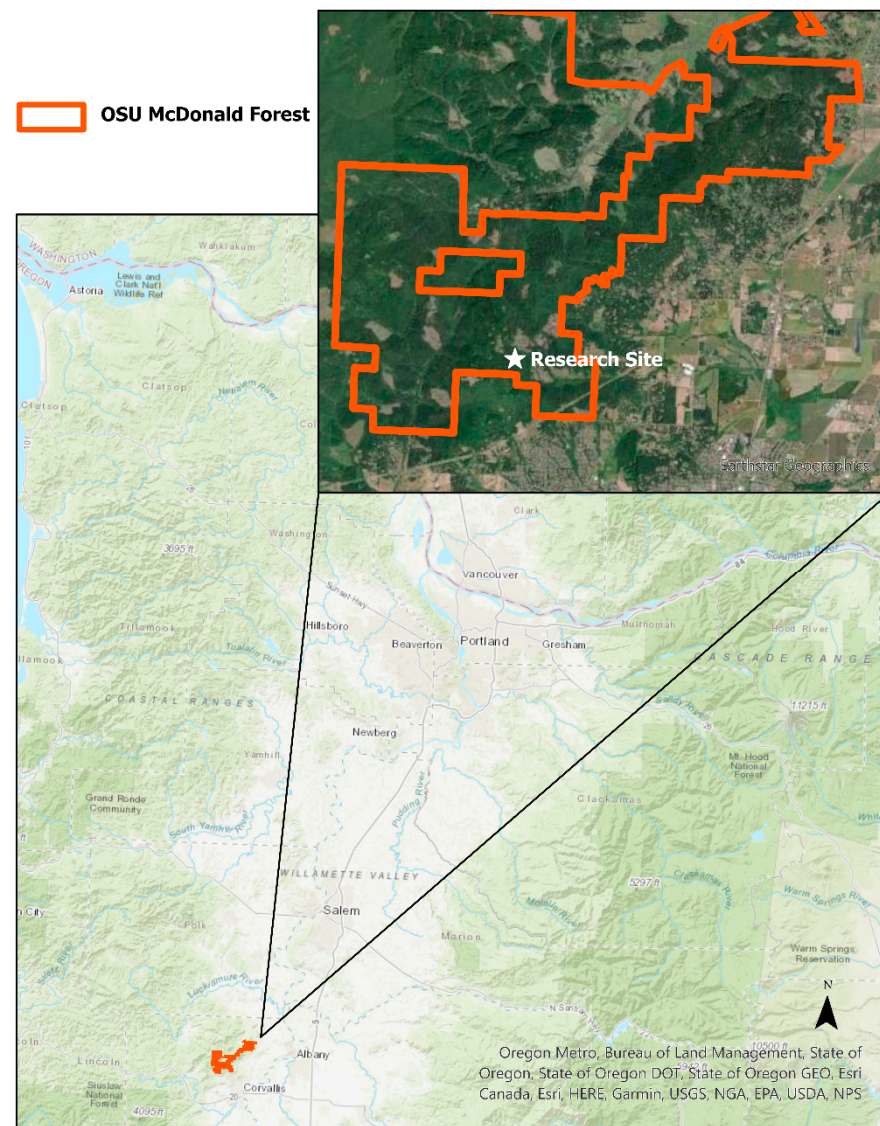


**Figure 1.** Vicinity map of OSU McDonald forest and research site.

Among the suite of software that implement SfM, we chose Agisoft Metashape Professional (version 1.6.2) to process the photos and generate photogrammetric point clouds (PPC). Metashape Professional reconstructs reality using side images. The majority of SfM software used in forestry are designed for a nadir view, whereas our study uses a perspective view, implemented only by a handful of software programs (e.g., Agisoft Metashape, 3DF Zephyr, and VisualSFM). We automatically aligned the photos using the unaltered

image (no downscaling) with up to 150,000 key points and 100,000 tie points. In some cases, the ‘generic preselection’ and ‘reference preselection’ options were used to improve image alignment. Agisoft Metashape did not align all photosets entirely, and it was necessary to retain separate tree sections (called ‘chunks’ in Agisoft). This automatic alignment process produced one to three ‘chunks’ per tree.

**Table 1.** Damage and location codes used in field data collection. Location codes refer to positions along the total height of the tree stem, divided into thirds.

Damage Code One	General Damage	Damage Code Two	Specific Damage	Location Code	Damage Location		
0	No Damage	0	No Damage	1	Bottom Third		
				2	Middle Third		
1	Unknown	0	Unknown	3	Top Third		
				2	Mechanical	1	Fire
							Logging
3	Chemical	1	Herbicide				
4	Disease	0	Unknown	1	Mistletoe		
				2	Needle rusts		
				3	Stem decay		
				4	Stem rusts		
				5	Stem chancre		
5	Insects	1	Defoliators	2	Bark beetles		
				3	Sucking insects		
				4	Pitch moths		
				6	Animal	1	Deer or elk
2	Bear						
3	Livestock						
4	Porcupine						
5	Mountain beaver						
7	Weather	1	Windthrow	2	Snow, ice, freeze		
				3	Drought		
				4	Lightning		
				5	Flooding		
				8	Suppression	0	Suppression
9	Physical	0	Butt swell	1	Broken top		
				2	Dead top		
				3	Multiple tops		
				4	Forked tree		
				5	Leaning tree		
				6	Crook or sweep		
				7	Seam or crack		
				8	Spike knot		
				9	Other		

Following alignment, we generated dense point clouds for all ‘chunks’ using the unaltered image and ‘high’ setting in Agisoft. We used the software Cloud Compare (version 2.10.2) to clean obvious, erroneous points within the PPC and to merge different sections of the same tree. We accomplished this by using distinct features on the tree stems as additional tie points. For instance, many trees contained unique, visible tree defects or painted tree numbers for this study.

Each PPC was scaled using the field-measured DBH and its corresponding height (1.37 m). In the unscaled point cloud, we measured a series of diameter and heights to find where the ratio of field DBH to height (1.37 m) is located. We computed the model scale

by dividing the field-measured DBH (m) by the model DBH (unscaled units), which was subsequently applied to the  $x$ ,  $y$ , and  $z$  of each point in the point cloud.

### 2.2.3. Handheld Lidar

In September of 2020, each plot was scanned with a GeoSLAM Zeb Horizon (Figure 2) handheld LiDAR unit (Nottingham, UK), equipped with a Velodyne VLP-16 sensor (San Jose, CA, USA). The LiDAR sensor operates 16 channels, spread uniformly to cover a field of view of  $30^\circ$  ( $\pm 15^\circ$ ), and sends 300,000 beams per second. The sensor can capture laser returns from a 100-m range (GeoSLAM), but previous work showed that the usable range is at most 60 m [21]. We walked the outside perimeter of each plot in an approximate circular pattern. The walking speed was normal to fast-paced. No targets or control points were placed within the scene. Each plot was scanned in less than two minutes.



**Figure 2.** Scanning in McDonald research forest using the GeoSLAM Zeb Horizon.

The point clouds acquired with the GeoSLAM Zeb Horizon were processed with GeoSLAM HUB 6.1 (GeoSLAM 2021), which uses a simultaneous localization and mapping (SLAM) algorithm to position the data. The software automatically refines and locates the position of the LiDAR unit and simultaneously generates the point cloud. Because the objective of the study was not to position the point clouds on the Earth, we used the local coordinate system rather than a global one.

### 2.3. Point Cloud Measurements

We estimated the tree dimensions and defect occurrence, type, and size on both photogrammetric and LiDAR point clouds using Cloud Compare (Table 2). The linear dimensions were estimated using the point-to-point linear distance feature, whereas qualitative attributes, such as damage type, were estimated visually from the point cloud. The same person performed all estimations, numerical and visual.

**Table 2.** Descriptions of point cloud measurements derived from handheld LiDAR and Structure from Motion (SfM) photogrammetry.

Measurement	Model	Type of Measurement	Units	Methodology
DBH	LiDAR	Linear	Meter	<ul style="list-style-type: none"> <li>• Horizontal measurement of diameter;</li> <li>• Taken approximately 1.37 m above ground-level;</li> <li>• Dimensions taken for three diameters <math>\sim 120^\circ</math> apart;</li> <li>• Average of three measures.</li> </ul>
Model Height	SfM	Linear	Meter	<ul style="list-style-type: none"> <li>• Vertical measurement of useable model height;</li> <li>• Taken from approximate ground-level to point where upper stem diameter is still visible in point cloud.</li> </ul>
Damage Type	SfM, LiDAR	Qualitative	None	<ul style="list-style-type: none"> <li>• Visual assessment of tree defect;</li> <li>• Assessed within the useable model height;</li> <li>• Recorded damage code according to Table 1.</li> </ul>
Damage Location	SfM, LiDAR	Linear	None	<ul style="list-style-type: none"> <li>• If defect is present, measured height to damage (from approximate ground-level) and recorded location according to Table 1;</li> <li>• Informed by field-measured total tree height.</li> </ul>
Damage Length	SfM, LiDAR	Linear	Meter	<ul style="list-style-type: none"> <li>• Vertical measurement of damage length</li> <li>• Approximate length of tree bole affected by the damage;</li> </ul>
Damage Count	SfM, LiDAR	Qualitative	None	<ul style="list-style-type: none"> <li>• Sum of the total number of damages per tree.</li> </ul>

## 2.4. Data Analysis

To answer the two research questions, we used linear mixed effects regression models:

$$y = X\beta + Z\gamma + \epsilon \quad (1)$$

where:

$y$  = subject's response vector (observed);

$X$  = fixed effects design matrix (known);

$\beta$  = fixed effects parameter vector (unknown);

$Z$  = random effects design matrix (known);

$\gamma$  = random effects parameter vector (unknown);

$\epsilon$  = vector of independent (Gaussian), random errors (unobserved).

For research question one (i.e., ability to detect damages), the response variable ( $y$ ) corresponded to total damage count per tree, whereas for the second research question (i.e., ability to estimate the magnitude of the damage), the response variable ( $y$ ) corresponded to damage length. The fixed effects ( $X$ ) were survey method and plot number (and damage type for research question two), while the random effect ( $Z$ ) was the tree number. We used multiple comparisons Scheffe's test to assess the differences among the levels of the fixed effects.

## 3. Results

### 3.1. Point Clouds

Of the 35 trees captured with handheld LiDAR and SfM, three did not produce point clouds that could be used for measurements. One of the failed trees was from a LiDAR point cloud (DBH 46 cm), and two were from the PPC (DBH 26 cm and 24 cm).

We computed root-mean-square-error (RMSE) and bias for the LiDAR-based estimates by comparing the LiDAR-derived DBH to field-measured DBH. The bias varied from  $-0.60$  to  $0.91$  cm, whereas the RMSE varied from  $1.00$  to  $4.04$  cm (Table 3). The RMSE and bias could not be calculated for the photogrammetric point clouds because they were scaled directly from the field DBH measurements (Section 2.2.2.).

**Table 3.** LiDAR root-mean-square-error and bias for DBH measurements on trees in three,  $400 \text{ m}^2$ , fixed-radius forest inventory plots.

Plot	RMSE (cm)	Bias (cm)
1	1.89	0.79
2	1.00	$-0.60$
3	4.04	0.91

The LiDAR point clouds had mean surface densities that varied from 7033 to 11,425 points per  $\text{m}^2$  (Figure 3). Surface density was not a valid metric for the photogrammetric point clouds; instead, we computed the mean number of points per tree. The photogrammetric point clouds had mean densities of 1,269,262 to 1,602,534 points per tree (Figure 4). For comparison, we also computed mean points per tree for the LiDAR models; they ranged from 295,805 to 710,130 points per tree (Table 4).

### 3.2. Damage Count and Length

Survey method and plot had significant effects on mean total damage count per tree ( $p$ -value =  $0.003$  and  $p$ -value =  $0.009$ , respectively), as visual estimates (1.62 damages per tree) were almost double the LiDAR and SfM values (0.93 damages per tree) (Table 5). Plots 1 and 2 had higher mean total damage counts per tree (1.39 and 1.42 damages per tree, respectively) compared to Plot 3 (0.66 damages per tree) (Table 5).

Survey method and plot number did not have a significant effect on mean damage length per tree ( $p$ -value =  $0.584$  and  $0.896$ , respectively). Estimated mean damage length



varied from 2.30 m (SE = 0.41) to 2.69 m (SE = 0.34) for the survey methods and from 2.43 m (SE = 0.33) to 2.59 m (SE = 0.33) across the three plots (Table 6). However, the type of damage had a significant effect on mean damage length per tree ( $p$ -value < 0.0001), which varied from 0.91 m (SE = 0.35, damage type = spike knot) to 8.61 m (SE = 1.56, damage type = multiple tops).

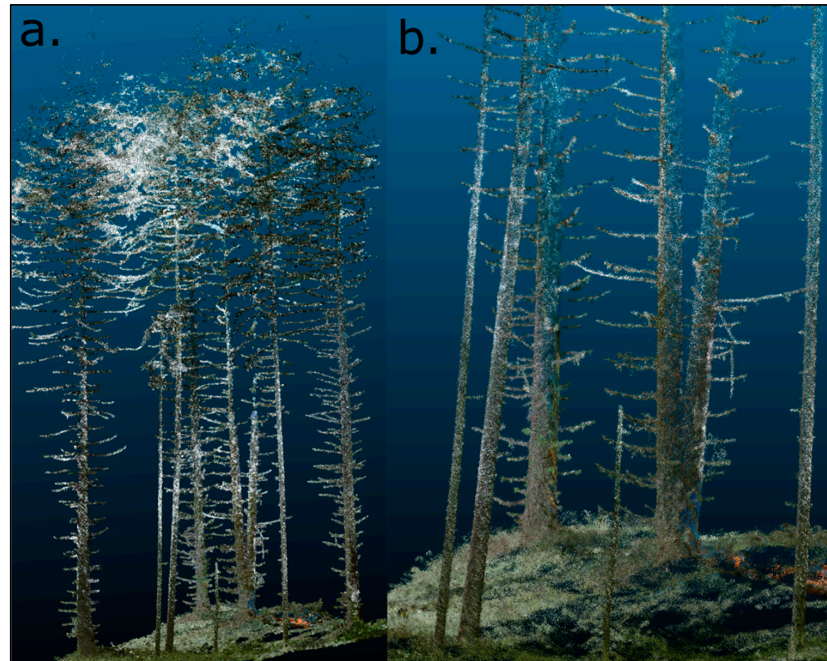


**Figure 3.** Handheld LiDAR model for plot three: (a) extent and (b) detail.

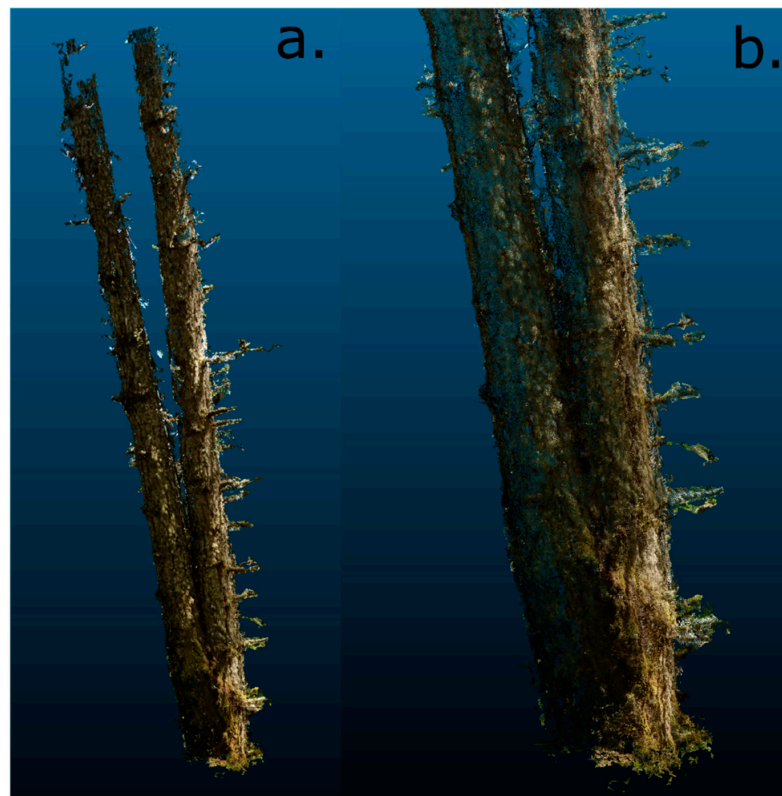


**Figure 4.** Sample photogrammetric point cloud for a tree in plot three developed with Structure from Motion: (a) whole tree extent and (b) detail.

**Table 4.** Mean point cloud density from handheld LiDAR and Structure from Motion (SfM) photogrammetry of three, 400 m<sup>2</sup> fixed-radius forest inventory plots.

Plot	Handheld LiDAR Point Cloud Density (Mean Points per m <sup>2</sup> )	Handheld LiDAR Point Cloud Density (Mean Points per Tree)	SfM Point Cloud Density (Mean Points per Tree)
1	7033	295,805	1,269,262
2	11,425	478,417	1,602,534
3	10,212	710,130	1,455,675

**Table 5.** Mean total damage count (per tree) comparing visual inventory, handheld LiDAR, and PPC-based methods of assessing tree damage.

Type 3 Tests of Fixed Effects			Least Squares Means	
Effect	<i>p</i> -Value	Effect	Estimate	Standard Error <sup>1</sup>
Method	0.003	Visual	1.62	0.21 (a)
		LiDAR	0.93	0.21 (b)
		PPC	0.93	0.21 (b)
Plot	0.009	Plot 1	1.39	0.20 (a)
		Plot 2	1.42	0.21 (a)
		Plot 3	0.66	0.26 (b)

<sup>1</sup> Least squares means estimates that do not share a letter are significantly different for the type three test of fixed effects at a 5% level of significance.

**Table 6.** Mean damage length (m) per tree comparing visual inventory, handheld LiDAR, and PPC-based methods of assessing tree damage.

Type 3 Tests of Fixed Effects			Least Squares Means	
Effect	<i>p</i> -Value	Effect <sup>1</sup>	Estimate	Standard Error <sup>2</sup>
Method	0.584	Visual	2.69	0.34
		LiDAR	2.30	0.41
		PPC	2.49	0.38
Plot	0.896	Plot 1	2.59	0.33
		Plot 2	2.43	0.33
		Plot 3	2.47	0.52
Damage Code	<0.0001	43	6.21	0.81 (a)
		45	1.82	0.44 (bc)
		52	1.60	1.56 (abc)
		90	1.83	0.70 (abc)
		91	1.04	0.79 (bc)
		93	8.61	1.56 (ab)
		94	1.56	0.40 (bc)
		95	1.60	1.57 (abc)
		96	1.31	0.30 (c)
		97	2.13	0.80 (abc)
98	0.91	0.35 (c)		
99	1.34	1.10 (abc)		

<sup>1</sup> Damage Codes: 43 = stem decay, 45 = stem canker, 52 = bark beetles, 90 = butt swell, 91 = broken top, 93 = multiple tops, 94 = fork, 95 = leaning, 96 = sweep, 97 = seam, 98 = spike knot, and 99 = other physical damage,

<sup>2</sup> Least squares means estimates that do not share a letter are significantly different for the type three test of fixed effects at a 5% level of significance.

## 4. Discussion

### 4.1. Damage Count

For the trees included in this study, we found convincing evidence of a significantly different total damage count between survey methods (*p*-value = 0.003). The two remote sensing methods appear to omit damage counts compared to the visual field method, as the

visual method estimated nearly twice as many damages per tree (mean = 1.62, SE = 0.21) than LiDAR and PPC-based methods (mean = 0.93, SE = 0.21).

These results support our hypothesis that the remote sensing methods would underestimate the damages compared to the visual field estimate. However, the evidence would be more convincing if specific damages and their positions were integrated into the fixed effects model and a similar result found. It is difficult to discern if the survey methods are including or omitting the same damage when looking at mean damage count per tree. Unfortunately, our sample data did not include enough damage counts from each damage code to support that type of analysis.

A limited number of studies used stationary terrestrial laser scanning (TLS) to assess tree damage and defect (18–20). Nguyen et al. (2020) used an automatic segmentation method and found ~98% of defects can be detected by TLS; however, there was also a very high number of false positives reported [18]. In contrast, our results show a higher level of omission than the Nguyen et al. (2020) [18]. The lower damage counts associated with our remote sensing methods were likely driven by the limited point cloud reconstruction of the upper stem section of the trees. For the 32 trees included in our study, the average field-measured height was 31.2 m, whereas LiDAR models captured an average useable height of 13.6 m, and the PPC-based models captured only 9.3 m. Therefore, the point cloud models reconstructed solely the lower third to half of the tree stem at the quality needed to detect tree damages. Piermattei et al. (2019) assessed the ability of SfM photogrammetry to derive forest inventory data; the maximum reconstructed tree heights in their study varied from 4.3 to 11.3 m [15]. Additionally, Fang and Strimbu (2017) found loblolly pine trees, modelled using SfM, could be used for diameter measurement up to ~13 m in height [8]. Bauwens et al. (2016) captured a maximum height of 24.6 m with a GeoSLAM ZEB1 handheld LiDAR sensor; however, TLS scans of the same trees reported maximum heights in the 40 to 45 m range [22]. Consequently, some handheld LiDAR sensors seem to capture at most two thirds of tall trees [22]. Other studies using a GeoSLAM ZEB Horizon sensor, like the one used in our research, had the maximum reconstructed heights ranging from 28 to 33 m [10,23]. Our LiDAR models captured points in the upper canopy of trees; however, only the lower segment of the tree stem was suitable for detecting tree damage.

Branches, leaves, and canopies of neighboring trees obscure the upper tree stem and make point cloud reconstruction difficult at greater heights. Panagiotidis et al. (2016) compared the accuracy of SfM-derived point clouds against terrestrial LiDAR point clouds and found that error increased linearly with height [24]. The authors noted that increased error likely occurs because of higher crown density, fewer points, and longer distances from the sensor to target object [24]. These factors probably limited the effective height of LiDAR and SfM-based stem models in our study as well, leading to reduced damage counts compared to visual methods, which were able to assess a larger proportion of the stem.

In addition to height limitations, environmental variables heavily influence the quality of point cloud models, particularly the PPC. For instance, light conditions varied from slightly overcast to sunny when we took photos of the trees, and some of the photos had heavy shadowing due to back-lighting of the trees on sunny days. Consistent light conditions, i.e., overcast weather days, likely provide better conditions for image acquisition that are subsequently used in the generation of PPC using SfM [9].

It is also possible that some of our failed tree models resulted from occlusion and related issues. For our study, LiDAR reconstructed 97% of the surveyed trees, and SfM reconstructed 94% of the surveyed trees. Piermattei et al. (2019) found SfM detected 65–98% of the target trees on a plot, with missing trees typically having DBHs less than 12 cm [15], significantly smaller than the missed trees in our study (i.e., measured DBH was 46 cm for LiDAR, and 26 cm and 24 cm for SfM). In our study, neighboring trees sometimes obscured the view to the target tree and forced the usage of pictures located at farther distances from the tree. Research suggests the angle between adjacent photos should not exceed 15–30 degrees [25]. For our missing trees, it is possible the angle between photos was too

large, and, as a result, the Agisoft software could not find enough tie points to create the point clouds.

Finally, the distance to the target tree varied, and it is possible that some photos were too far from the target object for ideal model reconstruction. Akpo et al. (2020) compared SfM models captured at distances of 1–5 m from the target tree [25]. They found the most accurate SfM models used images captured 1–2 m from the tree. Due to working with tall Douglas-fir trees, ranging from 15 to 42 m in height, our photos were captured approximately 5–10 m from the target to maximize the length of tree stem captured in a photo. At this distance, we may have captured more tree stem, but potentially lost resolution and quality in our SfM models compared to images captured closer to the target stem.

To expand on this work in future studies, we recommend including a sufficient number of observations per unique damage code type. Additionally, researchers may want to identify the exact position of the damage, such as stem height at the start and end of the damage. Finally, higher quality photogrammetric point cloud models may be obtained with better image quality—aided by newer smartphone cameras, lenses with wider field of view, consistent and overcast ambient light conditions, and optimal distance to the target object.

#### 4.2. Damage Length

For the trees included in our study, there is no evidence that damage length varied between survey methods ( $p$ -value = 0.584). The estimates of mean damage length per tree were not significantly different from one another (Visual = 2.69 m, LiDAR = 2.30 m, and SfM = 2.49 m), which support our hypothesis that handheld LiDAR and SfM photogrammetry can quantify damage length, similar to traditional field methods.

Our findings are consistent with other accuracy assessments of handheld LiDAR and SfM; to date, many of the forest inventory studies for these two methods have focused on DBH-derived measures. In a review of the current literature, Iglhaut et al. (2019) found RMSEs for SfM-derived DBH ranged from 0.9 to 6.8 cm, compared to field or TLS DBH measurements [9]. Additionally, Piermattei et al. (2019) found no significant difference between field, SfM, and terrestrial LiDAR measures of DBH [15]. Handheld LiDAR can also produce DBH estimates with high accuracy—on the order of 1.1 cm RMSE [22]. Finally, Huang et al. (2018) found the accuracy and completeness of SfM models to be comparable with TLS models [26]. In their research, SfM point clouds had standard deviations of 0.009 to 0.02 m for point-to-point distance compared to a TLS cloud. Our results agree with the existing literature and find handheld LiDAR and SfM capable of measuring linear features with high accuracy.

Although the use of a scale bar or target for scaling the SfM measurements could potentially produce more accurate estimates of size-related variables, such as damage length, Liang et al. (2014) demonstrated that natural objects can be used to generate accurate scaling of photogrammetric point clouds [10]. The manual alignment of a limited number of point cloud chunks from Agisoft Metashape within CloudCompare could also introduce error, but a similar process was shown to produce highly accurate (i.e., <1–5 mm) estimates of changes in size (i.e., growth) in complex, branching coral structures [27]. Since previously reported errors of less than 1 mm [27] for manually aligned point cloud chunks are orders of magnitude smaller than the dimensional measurements of interest in this study (e.g., tens to hundreds of cm for tree diameters and damage length), they are unlikely to have impacted our conclusions. Further, the lack of significant differences among mean damage length estimates from our visual, SfM, and LiDAR methods and consistency of our accuracy assessments with RMSE estimates reported in other studies suggests that the scaling method we used for SfM, which was based on field-measured diameters at 1.37 m, is likely sufficient for measuring many tree damages. However, future explorations of the application of SfM to tree damage detection and measurement might benefit from the use of coded targets, which increase the reliability of the image alignment process [28], reducing the need to manually align separate point cloud chunks in CloudCompare.

Finally, the results of our study could be strengthened by destructive field sampling. For instance, sample trees could be felled and the exact length of the damage measured with a distance tape. This would eliminate problems associated with visual estimation and measurement errors from laser rangefinders, clinometers, relaskops, etc., and provide a means to directly compare the accuracy of field defect detection methods with handheld LiDAR and PPC-based methods.

## 5. Conclusions

This study evaluated the ability of two remote sensing methods to detect and quantify common tree damages. Our results largely support the hypothesis that handheld LiDAR and ground-based PPC omit tree defects compared to visual field estimates. We found a significantly different mean damage count per tree between the three survey methods, with the field method recording nearly twice as many damages per tree as the handheld LiDAR and SfM methods. The remote sensing methods likely omit damages due to occlusion and environmental variables, such as variable lighting conditions. There were also a few instances where distance between photo points and distance to the target tree were longer than desired. Additionally, our results support the hypothesis that handheld LiDAR and PPC can quantify damage length in a manner similar to field methods. For the trees included in our study, there was no evidence that damage length varied between the three survey methods. These findings are consistent with other accuracy assessments of linear tree measurements conducted via handheld LiDAR and SfM [9,15,22,26].

This research was designed as an introductory step in detecting and quantifying tree damages with handheld LiDAR and SfM photogrammetry. More research is needed to replicate and improve upon this work in different regions and forest types. The natural expansion of our study is to use handheld LiDAR and SfM to automatically detect, classify, and measure tree defects. We believe this is essential research and required to integrate mobile remote sensing methods into active forest inventory programs.

**Author Contributions:** Conceptualization, C.J.M. and B.M.S.; methodology, C.J.M., M.P. and B.M.S.; software, C.J.M. and B.M.S.; validation, C.J.M. and B.M.S.; formal analysis, C.J.M.; investigation, C.J.M.; resources, C.J.M., M.P. and B.M.S.; data curation, C.J.M.; writing—original draft preparation, C.J.M.; writing—review and editing, M.P. and B.M.S.; visualization, C.J.M.; supervision, M.P.; project administration, M.P. and B.M.S.; funding acquisition, M.P. and B.M.S. All authors have read and agreed to the published version of the manuscript.

**Funding:** This research was funded by Oregon State University's Department of Forest Engineering, Resources and Management, and the Oregon State University College of Forestry Research Forests.

**Data Availability Statement:** Data available on request.

**Acknowledgments:** We would like to thank Stephen Fitzgerald for providing feedback on an earlier draft of this manuscript, and Nicholas Bryant and Dylan Johnson for assisting with field data collection.

**Conflicts of Interest:** The authors declare no conflict of interest. The funders had no role in the design of the study; in the collection, analyses, or interpretation of data; in the writing of the manuscript, or in the decision to publish the results.

## References

1. Natural Resources Conservation Service. *Forestry Technical Note No. FOR-1: Forest Inventory Methods*; USDA: Washington, DC, USA, 2018.
2. Bragg, D.C. An improved tree height measurement technique tested on mature southern pines. *South. J. Appl. For.* **2008**, *32*, 38–43. [[CrossRef](#)]
3. Kitahara, F.; Mizoue, N.; Yoshida, S. Effects of training for inexperienced surveyors on data quality of tree diameter and height measurements. *Silva Fenn.* **2010**, *44*, 657–667. [[CrossRef](#)]
4. Donager, J.J.; Meador, A.J.S.; Blackburn, R.C. Adjudicating perspectives on forest structure: How do airborne, terrestrial, and mobile lidar-derived estimates compare? *Remote Sens.* **2021**, *13*, 2297. [[CrossRef](#)]
5. Gollob, C.; Ritter, T.; Nothdurft, A. Forest inventory with long range and high-speed personal laser scanning (PLS) and simultaneous localization and mapping (SLAM) Technology. *Remote Sens.* **2020**, *12*, 1509. [[CrossRef](#)]

6. Hyyppä, E.; Yu, X.; Kaartinen, H.; Hakala, T.; Kukko, A.; Vastaranta, M.; Hyyppä, J. Comparison of backpack, handheld, under-canopy UAV, and above-Canopy UAV laser scanning for field reference data collection in boreal forests. *Remote Sens.* **2020**, *12*, 3327. [[CrossRef](#)]
7. GeoSLAM. ZEB Horizon. Available online: <https://geoslam.com/solutions/zeb-horizon> (accessed on 10 October 2021).
8. Fang, R.; Strimbu, B.M. Stem measurements and taper modeling using photogrammetric point clouds. *Remote Sens.* **2017**, *9*, 716. [[CrossRef](#)]
9. Iglhaut, J.; Cabo, C.; Puliti, S.; Piermattei, L.; O'Connor, J.; Rosette, J. Structure from Motion photogrammetry in forestry: A review. *Curr. For. Rep.* **2019**, *5*, 155–168. [[CrossRef](#)]
10. Liang, X.; Jaakkola, A.; Wang, Y.; Hyyppä, J.; Honkavaara, E.; Liu, L.; Kaartinen, H. The use of a hand-held camera for individual tree 3D mapping in forest sample plots. *Remote Sens.* **2014**, *6*, 6587–6603. [[CrossRef](#)]
11. Mikita, T.; Janata, P.; Surový, P. Forest stand inventory based on combined aerial and terrestrial close-range photogrammetry. *Forests* **2016**, *7*, 165. [[CrossRef](#)]
12. Surový, P.; Yoshimoto, A.; Panagiotidis, D. Accuracy of reconstruction of the tree stem surface using terrestrial close-range photogrammetry. *Remote Sens.* **2016**, *8*, 123. [[CrossRef](#)]
13. Liu, J.; Feng, Z.; Yang, L.; Mannan, A.; Khan, T.; Zhao, Z.; Cheng, Z. Extraction of sample plot parameters from 3D point cloud reconstruction based on combined RTK and CCD continuous photography. *Remote Sens.* **2018**, *10*, 1299. [[CrossRef](#)]
14. Mokroš, M.; Liang, X.; Surový, P.; Valent, P.; Čerňava, J.; Chudý, F.; Tunák, D.; Saloň, Š.; Merganič, J. Evaluation of close-range photogrammetry image collection methods for estimating tree diameters. *ISPRS Int. J. Geo-Inform.* **2018**, *7*, 93. [[CrossRef](#)]
15. Piermattei, L.; Karel, W.; Wang, D.; Wieser, M.; Mokroš, M.; Surový, P.; Koreň, M.; Tomaščík, J.; Pfeifer, N.; Hollaus, M. Terrestrial Structure from Motion photogrammetry for deriving forest inventory data. *Remote Sens.* **2018**, *11*, 950. [[CrossRef](#)]
16. Raunonen, P.; Greco, R.; Persia, M.; Tartarino, P.; Marzulli, M.I. Estimating tree stem diameters and volume from smartphone photogrammetric point clouds. *Forestry* **2020**, *93*, 411–429.
17. Bell, J.F.; Dilworth, J.R. *Log Scaling and Timber Cruising*; John Bell & Associates, Inc.: Corvallis, OR, USA, 2007; 397p.
18. Nguyen, V.-T.; Constant, T.; Kerautret, B.; Debled-Rennesson, I.; Colin, F. A machine-learning approach for classifying defects on tree trunks using terrestrial LiDAR. *Comput. Electron. Agric.* **2020**, *171*, 105332. [[CrossRef](#)]
19. Stangle, S.M.; Brochert, F.; Kretschmer, U.; Spiecker, H.; Sauter, U.H. Clear wood content in standing trees predicted from branch scar measurements with terrestrial LiDAR and verified with X-ray computed tomography. *Can. J. For. Res.* **2014**, *44*, 145–153. [[CrossRef](#)]
20. Mengesha, T.; Hawkins, M.; Tarleton, M.; Nieuwenhuis, M. Stem quality assessment using terrestrial laser scanning technology: A case study of ash trees with a range of defects in two stands in Ireland. *Scand. J. For. Res.* **2015**, *30*, 605–616. [[CrossRef](#)]
21. Garms, C.G.; Strimbu, B.M. Impact of stem lean on estimation of Douglas-fir (*Pseudotsuga menziesii*) diameter and volume using mobile lidar scans. *Can. J. For. Res.* **2021**, *51*, 1117–1130. [[CrossRef](#)]
22. Bauwens, S.; Bartholomeus, H.; Calders, K.; Lejeune, P. Forest inventory with terrestrial LiDAR: A comparison of static and hand-held mobile laser scanning. *Forests* **2016**, *7*, 127. [[CrossRef](#)]
23. Jurjević, L.; Liang, X.; Gašparović, M.; Balenović, I. Is field-measured tree height as reliable as believed—Part II, A comparison study of tree height estimates from conventional field measurement and low-cost close-range remote sensing in a deciduous forest. *ISPRS J. Photogramm. Remote Sens.* **2020**, *169*, 227–241. [[CrossRef](#)]
24. Panagiotidis, D.; Surový, P.; Kuželka, K. Accuracy of Structure from Motion models in comparison with terrestrial laser scanner for the analysis of DBH and height influence on error behaviour. *J. For. Sci.* **2016**, *62*, 357–365. [[CrossRef](#)]
25. Akpo, H.A.; Atindogbé, G.; Obiakara, M.C.; Adjinanoukon, A.B.; Gbedolo, M.; Lejeune, P.; Fonton, N.H. Image data acquisition for estimating individual trees metrics: Closer is better. *Forests* **2020**, *11*, 121. [[CrossRef](#)]
26. Huang, H.; Zhang, H.; Chen, C.; Tang, L. Three-dimensional digitization of the arid land plant *Haloxylon ammodendron* using a consumer-grade camera. *Ecol. Evol.* **2018**, *8*, 5891–5899. [[CrossRef](#)] [[PubMed](#)]
27. Lange, I.D.; Perry, C.T. A quick, easy and non-invasive method to quantify coral growth rates using photogrammetry and 3D model comparisons. *Methods Ecol. Evol.* **2020**, *11*, 714–726. [[CrossRef](#)]
28. Krisanski, S.; Taskhiri, M.S.; Turner, P. Enhancing methods for under-canopy unmanned aircraft systems based photogrammetry in complex forests for tree diameter measurement. *Remote Sens.* **2020**, *12*, 1652. [[CrossRef](#)]